THE JOURNAL OF PHYSICAL CHEMISTRY B

Article

pubs.acs.org/JPCB

Composition Dependence of the Micellar Architecture Made from Poly(ethylene glycol)-*block*-Poly(partially benzyl-esterified aspartic acid)

Yusuke Sanada, Isamu Akiba, Satoshi Hashida, and Kazuo Sakurai*

Department of Chemistry and Biochemistry, The University of Kitakyushu, 1-1 Hibikino, Wakamatsu-ku, Kitakyushu, Fukuoka 808-0135, Japan

Kouichi Shiraishi and Masayuki Yokoyama

Medical Engineering Laboratory, Research Center for Medical Science, Jikei University School of Medicine, 3-25-8 Nishi-shinbashi, Minato-ku, Tokyo 105-8461, Japan

Naoto Yagi

Japan Synchrotron Radiation Research Institute (JASRI/SPring-8), 1-1-1 Kouto, Sayo, Hyogo 679-5198, Japan

Yuya Shinohara and Yoshiyuki Amemiya

Department of Advanced Materials Science, Graduate School of Frontier Sciences, The University of Tokyo, 5-1-5 Kashiwanoha, Kashiwa, Chiba 277-8561, Japan

Supporting Information

ABSTRACT: Poly(ethylene glycol)-*block*-poly(partially benzyl-esterified aspartic acid), denoted by PEG-P(Asp(Bzl)), is one of the most examined blockcopolymers for drug carriers. However, little is known about fundamental physical properties. Nine samples of PEG-P(Asp(Bzl)) with different benzylation fractions (F_{Bzl}) and aspartic chain lengths (DP_{Asp}) were synthesized, and the aggregation number (N_{agg}), core radius (R_C), and other structural parameters were determined with combination of light scattering and synchrotron X-ray small-angle scattering. The major factor to determine N_{agg} and R_C was found to be F_{Bzl}, i.e., the hydrophobic nature of the core, even though F_{Bzl} was changed in the relatively small composition range from 66 to 89 mol %. When we compared the data for the same F_{Bzl}, the scaling theory was consistent with the core chain length dependence of both core and micelle sizes. The overcrowding nature of the tethered PEG chains on the micelles was increased about 1.3−2.9 times with increasing N_{agg} compared with the unperturbed state in solutions.

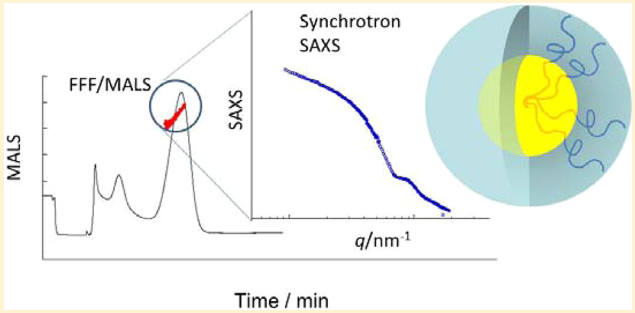

INTRODUCTION

Amphiphilic blockcopolymers can self-assemble into a spherical micelle with core−shell architecture in aqueous solutions. Here, the hydrophobic blocks are segregated from water to form a densely packed core that can encapsulate hydrophobic compounds, while the hydrophilic blocks can be dissolved in water and thus form a diffuse and soft interface with water. These micelles are called polymeric micelles and play an important role in drug delivery systems (DDSs)[1−4] and other applications such as nanotemplates[3−5] and surface modification tools by use of the tethered hydrophilic chains on their surface.[5] Eisenberg et al.[6−10] and other groups[11] demonstrated that the morphology of blockcopolymer aggregates depends a great deal on the solvent polarity, pH, and salt concentration and shows surprisingly rich variations in shape. Kataoka and Kabanov are the major contributors to apply polymeric micelles into DDS.[3,12−16] Among these novel systems, several polymeric micelles incorporating anticancer drugs are under clinical evaluation,[17,18] and they fall in the category of biocompatible copolymers consisting of poly(ethylene glycol) (PEG) and hydrophobic polypeptide. Among others, poly(ethylene glycol)-*block*-poly(partially benzyl-esterified aspartic acid), denoted by PEG-P(Asp(Bzl)), is one of

Received: January 29, 2012
Revised: June 6, 2012
Published: June 11, 2012

   dx.doi.org/10.1021/jp300936d | *J. Phys. Chem. B* 2012, 116, 8241−8250

the most extensively examined blockcopolymers in terms of correlations between its chemical structures and the characteristics of drug carriers.[19]

The formation of the core−shell polymeric micelles from blockcopolymers can be understood in terms of the volumetric balance between the hydrophilic and hydrophobic groups. Additionally, we have to consider the following three factors: (1) the entropic elasticity of the core chains determined by R_C^2/R_e^2 where R_C and R_e are the core radius and the Gaussian end-to-end distance of the individual core block, (2) the interaction free energy of the shell chain's conformation given by the balance of the elastic stretching of the shell chain, the excluded volume effect between the monomers (repulsive interaction between the monomers), and the attractive solvent−monomer interactions, and (3) the interfacial tension between the core chains and the solvent molecules.[20−23] The free energy of the micellar formation is given by the balance of these factors. The relative significance of these three components is dependent on the chain length of the hydrophobic (N_C) and hydrophilic (N_S) blocks. For the case of $N_C < N_S$, stable core−shell micelles are formed and the osmotic free energy of the shell chains is expected to dominantly determine the micelle structures and the number of aggregation (N_{agg}).[20,23] Zhulina et al.[20] applied the scaling concepts[24,25] to core−shell spherical micelles to lead the power law dependence for the structural parameters, and recently, they elaborated their original theory.[21] It is interesting that when $N_C < N_S$ the micellar parameters such as the core radius and the aggregation number become almost independent of N_S and mainly determined by N_C.

Although those are not aqueous systems, a number of experimental studies confirmed the general features of the theoretical predictions.[20,22] In some cases, however, the measured values of the corresponding exponents deviate from the theoretical predictions and the discrepancies are considered as being due to slow kinetics of the micellar formation and molecular weight polydispersity.[22] Riley et al.[26] studied small-angle neutron scattering (SANS) from the polymer micelle solutions made from poly(lactic acid)-*b*-poly(ethylene glycol) (PLA-*b*-PEG) with a wide range of N_C/N_S ratios (ca., $M_{w,PLA}$:$M_{w,PEG}$ = 3:5, 15:5, 45:5, where $M_{w,PEG}$ was fixed at 5000). They found that the shell thickness and the PEG block conformation are strongly correlated with the PLA core size: the PEG segments are localized in the vicinity of the PLA/PEG interface in the smaller core; in contrast, they became more homogeneous along the radial direction in the case of the larger core. Their finding was consistent with the predictions. Additionally, including ourselves,[27] several groups studied the micelle structures with SANS and/or SAXS (small-angle X-ray scattering) and revealed these techniques are useful for in situ measurements of the polymeric micelles.[28−32]

The scattering from polymeric micelles consisting of a spherical core and several shell chains comprises four terms: the self-correlation of the core, the self-correlation of the shell chains, the cross-term between the core and the shell chains, and the cross-term between the shell chains. Therefore, to obtain the structural information from the analysis of SAXS or SANS, an appropriate statistical model for the shell chains is needed. Daoud and Cotton are the first to present a theory of multi-armed star polymers that can be used to describe the shell chain statistic.[25] Later, Pedersen and Svaneborg developed an elaborated general scattering theory for polymer micelles. They derived the form factors for two types of micelles:[33] noninteracting Gaussian chains with dilute shell region and interacting self-avoiding chains with well dense (but not highly stretched). Their theory is shown to well describe the scattering.[33,34]

In terms of DDS application, the asymmetric blockcopolymers with $N_C < N_S$ have been used to obtain stable micelles, especially for PEG-P(Asp(Bzl)). According to the previous papers, it was revealed that subtle differences in chemical structures of the blockcopolymers as well as of the loaded drugs result in substantial changes in drug delivering performance.[19,27] However, little is elucidated about what are the essential physicochemical factors to control DDS performance. One reason for such insufficient understanding is that very limited information has been obtained for the drug incorporating inner core. In most cases, only drug contents were measured, while the size of the inner core and drug distribution in the inner core have not been analyzed. Although its practical importance of clinical trial, it seems that little is known about how the chemical composition of the P(Asp(Bzl)) influences the micelle size. Controlling the particle sizes and inner structures is essentially important in DDS design. This paper presents synchrotron SAXS and light scattering studies on the PEG-P(Asp(Bzl)) micelle with different core chain lengths and chemical compositions to clarify the factors to determine its micellar architecture.

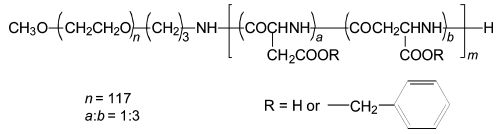

Figure 1. The chemical structure of poly(ethylene glycol)-*block*-poly(partially benzyl-esterified aspartic acid).

EXPERIMENTAL SECTION

Materials and Micelle Preparation. Nine samples of PEG-P(Asp(Bzl)) were newly synthesized for this study with ring-opening polymerization of β-benzyl L-aspartate *N*-carboxyanhydride (BLA-NCA) from a primary amino-terminated PEG with one end capped with a methoxy group, followed by a full hydration of the side chains and then partial benzylestrification, as described elsewhere.[12,35] The poly(amino acid) block was composed of a 1:3 (mol) mixture of the α-amide and β-amide aspartic acid residues owing to the alkaline hydrolysis procedure. By changing the feed ratio of BLA-NCA to the PEG from 25 to 39 (mol), the Asp block length (DP_{Asp}) was changed from 20 to 32 in terms of the degree of polymerization and the benzylation fraction (F_{Bzl}) was controlled by changing the feed ratio of phenyl methanol. The molecular characterization was done with ^{1}H NMR in DMSO-d_6 with 3 v/v % of TFA to determine DP_{Asp} and F_{Bzl}. Only when $0.6 < F_{Bzl} < 0.9$, we could obtain stable micelle solutions. At $F_{Bzl} > 0.9$, there was no micelle but large aggregates or precipitation were observed, and at $F_{Bzl} < 0.6$, there was no micelle formation and the products were apparently dissolved in water. The molecular characters are summarized in Table 1 as well as the sample codes used in this paper. In this paper, we use sample code such as A26.4-B76.9, in which the numbers after A and B represent the degree of polymerization of the Asp(Bzl) block denoted by DP_{Asp} and F_{Bzl}, respectively. In our synthesis, the amino-terminated PEG was supplied from NOF Corp. (Tokyo, Japan). Its weight average molecular weight was 5200, and its purity was more than 99.9%.

dx.doi.org/10.1021/jp300936d | J. Phys. Chem. B 2012, 116, 8241−8250

Table 1. Molecular Characters of Poly(ethylene glycol)-*block*-poly(partially benzyl-esterified aspartic acid) (PEG-P(Asp(Bzl)) Samples

lot code	polymer sample code[a]	Asp number (DP_{Aap})[b]	benzylation (F_{Bzl})[c] (%)	CMC[d] (μg mL^{-1})
HH9-31-1	A26.4-B76.9	26.4	76.9	4.0
HH9-31-2	A26.4-B81.4	26.4	81.4	4.0
HH9-24-2	A26.4-B88.6	26.4	88.6	4.0
HH9-22-2	A20.2-B83.7	20.2	83.7	6.3
HH9-22-4	A23.8-B84.0	23.8	84.0	4.5
HH9-22-3	A29.7-B82.2	29.7	82.2	5.0
HH9-22-5	A32.0-B77.2	32.0	77.2	
HH9-24-1	A26.9-B65.8	26.9	65.8	5.6
HH9-18-1	A26.9-B83.3	26.9	83.3	2.2

[a]The code represents the block composition. [b]Number of aspartate units determined with ^{1}H NMR. The α/β ratio was 1/3. [c]The benzylation fraction was determined with ^{1}H NMR. [d]The CMC was determined by the fluorescence method.[3]

β-Benzyl L-aspartate *N*-carboxyanhydride was synthesized from β-benzyl L-aspartate according to the conventional method.[19]

The obtained PEG-P(Asp(Bzl)) was dissolved in THF, and the THF was evaporated at 40 °C under N_2 flow. After being further dried under reduced pressure, the polymer was sonicated in 1× Dulbecco phosphate-buffered saline at 8.6 mg/mL with 5 mm diameter microtip of a VCX-750 sonicator (Sonic&-Materials Inc., CT, USA), and the obtained polymeric micelle solutions were centrifuged (3900 rpm, 10 min) to remove insoluble precipitates. We used a filter unit equipped with an Amicon Ultra-15 (MWCO = 100k) to concentrate the micelle solutions, and the micelle solutions were passed through a Millex 0.22 μm PVDF filter unit. Since even a small amount of secondary aggregation caused errors in scattering experiment, the sample solutions were sonicated with a UH-50 ultrasonic homogenizer (SMT Company) for at least 1 min before measurements. We confirmed that this procedure did not change the micelle size and other properties. Only for A26.9-B83.3, to examine how the different micelle preparation method affects the results, we made micelles by dialyzing the A26.9-B83.3/DMF solution with Dulbecco buffer and the concentration was determined with UV absorbance. The micellar samples were named adding -s (sonication) or -d (dialysis) at the end of the polymer code.

The critical micelle concentration (CMC) was determined for each polymer (except A32.0-B77.2) at 25 °C in the same buffer solution as mentioned above and found to be less than 0.007 mg/mL (Table 1).[3] These values were much lower than those used in the scattering experiments.

Field Flow Fractionation (FFF) Coupled with Light Scattering (LS). An Eclipse 3+ separation system (Wyatt Technology Europe, Dernbach, Germany) was used as FFF, which was sequentially connected to a Dawn Heleos II multiangle light scattering (LS) detector (Wyatt Technology) and an Optilab rEX DSP differential refractive index (RI) detector (Wyatt Technology) operating at a wavelength of 658 nm, in that order from the upper stream. A Wyatt channel (Eclipse 3 channel LC) was used, which has a tip-to-tip length of 17.4 cm and a nominal thickness of 250 μm, and a membrane (Nadir cellulose membrane 10 kDa LC) was attached on the bottom of the channel. An Agilent 1200 series isocratic pump (Agilent Technologies, Waldbronn, Germany) equipped with a Gastorr TG-14 in-line vacuum degasser (FLOM Co., Ltd.) was used to control the carrier flow and sample injection. Between the pump and the channel was placed a filter holder with a 100 nm pore size poly(vinylidene fluoride) membrane (Millipore Corp.) for optical purification. Dulbecco buffer was used as both the solvent and the eluent. The focusing point was positioned at 2 mm downstream from the inlet, and the cross-flow rate was controlled to decrease exponentially and the channel flow rate was fixed at 1 mL/min. All FFF/MALS measurements were carried out at 22−28 °C. As the standard procedure, a 30 μL sample solution of 10 mg/mL in concentration was supplied with an Agilent 1200 series autosampler (Agilent Technologies). When the injection concentration was changed to 3.0 mg/mL, the obtained results were identical within experimental error.

LS measurements were made at 25.0 °C with a vertically polarized Ga−As laser (658 nm) with a Dawn Heleos II, and the photometer was calibrated using pure toluene and aqueous solutions of low molecular weight dextran samples. Scattered light intensities at scattering angles over 14−163° were measured, and their angular dependence was analyzed using Berry's plot to determine the *Z*-average radius of gyration ($\langle S^2\rangle_Z^{1/2}$) and the weight averaged molecular mass (M_w) for each polymeric micelle (note that M_w means the molar mass of the aggregated micelles instead of the individual block-copolymer) by use of the following equation:

$$(Kc/R_\theta)_{c\to 0}^{1/2} = \frac{1}{M_w^{1/2}} + \frac{1}{6}\frac{\langle S^2\rangle_Z}{M_w^{1/2}}q^2 + O(q^4) \quad (1)$$

Here, K is the optical constant, c is the micelle mass concentration, R_θ is the reduced scattering intensity at scattering angle 2θ, and q is the magnitude of the scattering vector defined by $q = 4\pi \sin\theta/\lambda$. Since the concentration flowed into the LS detector was so low ($c < 0.2$ mg/mL) in the present setup that the concentration dependence of R_θ can be negligibly small, we analyzed the data regarding the obtained Kc/R_θ as $(Kc/R_\theta)_{c\to 0}$. The specific refractive index increment $(\partial n/\partial c)$ of the polymer micelles in Dulbecco buffer was determine for each sample with a DRM-1021 differential refractometer (Otuska Electronics), except for A23.8-B84.0-s, A29.7-B82.2-s, and A26.9-B65.8-s due to the limited amount of the samples. For those, $\partial n/\partial c$ was calculated from the relation of $\partial n/\partial c = w_1(\partial n/\partial c)_1 + w_2(\partial n/\partial c)_2 + w_3(\partial n/\partial c)_3 + ...$, where w_i is the weight fraction of each chemical composition of i and we used 1.378, 1.559, and 1.950 for $\partial n/\partial c$ of PEG, PAsp, and PBzlAsp, respectively. The obtained values were used to determine both c and K in eq 1. From the chemical composition given in Table 1, the molecular weight of one PEG-P(Asp(Bzl)) block, $M_{PEG\text{-}P(Asp(Bzl))}$, can be evaluated. Combining M_w and $M_{PEG\text{-}P(Asp(Bzl))}$, the weight-average aggregation number $N_{agg,w}$ can be determined by $N_{agg,w} = M_w/M_{PEG\text{-}P(Asp(Bzl))}$.

Synchrotron SAXS Measurements. SAXS measurements were performed at BL-40B2 of SPring-8, Japan. A 30 cm × 30 cm imaging plate (Rigaku R-AXIS VII) detector was placed at 0.75 or 1.65 m away from the sample. The wavelengths of the incident beam (λ) were 0.071 or 0.10 nm. The 0.75 and 1.65 m set-ups provided q ranges of 1.0−8.0 and 0.08−2.0 nm^{-1}, respectively. A bespoke SAXS vacuum sample chamber[27] was used, and the X-ray transmittance of the samples was determined with an ion chamber located in front of the sample and a Si photodiode for X-ray (Hamamatsu Photonics S8193) after the sample.

dx.doi.org/10.1021/jp300936d | J. Phys. Chem. B 2012, 116, 8241−8250

The micelle solutions were packed in a quart capillary (2 mm ϕ, Hilgenberg GmbH) or our special cell[36] and set in the sample chamber. SAXS from a sample solution was measured at an exposure time of 2 or 5 min. All SAXS measurements were carried out at 22−28 °C, and the temperature difference within this range did not change the scattering profiles at all and thus the results derived from them. The resulting two-dimensional SAXS images were converted to one-dimensional $I(q)$ vs q profiles by circular averaging. Here, $I(q)$ was the scattering intensity at q, and to obtain the excess scattering intensity by micelles, the background scatterings from the buffer and the cell were subtracted after an appropriate transmittance correction.[36,37] The subtractions were carried out for all samples without any ambiguity. The measured SAXS intensities were corrected to an absolute scale using the absolute scattering intensities of water of 1.632×10^{-2} cm^{-1} (see the Supporting Information).[38] The scattering experiments were carried out in the range 0.5 mg/mL < c < 2.0 mg/mL, and $[I(q)/c]_{c\to 0}$ was obtained for each q for all samples (see the Supporting Information). As a matter of fact, at q > 0.2 nm^{-1}, we did not observe the concentration dependence of $I(q)/c$. Sometimes, we observed an up-turn of the intensity at lower q, which can be ascribed to the presence of secondary aggregates of the micelles, rather than improper subtraction. The presence of the aggregates was confirmed with FFF (see Figure S3, Supporting Information). There was also an up-turn at high q observed, deviating from the Porod law. This can be due to the atomic nature of the material and to the density fluctuation at all size scales of atoms.[39]

Reproducibility and Equilibrium Issues. The present polymeric micelles were very stable in the temperature range 20−30 °C so that the SAXS profiles and the FFF chromatograms did not change even after the samples were left for a few days at r.t. From our preliminary experiment, there was no critical micelle temperature (CMT) observed below 60 °C, and the SAXS profiles did not depend on temperature in the range 20−30 °C. All SAXS measurements were carried out above the CMC. We examined reproducibility in scattering experiments. When the micelles were prepared with the same procedure from the same polymer sample but as a different lot, the discrepancy in the structural parameters such as the radius of the core of the micelle and N_{agg} was less than 5%. However, when we prepared them with a different procedure from the same polymer sample (such as sonication vs dialysis), the discrepancy became larger than 10%. Since we carried out our measurements far above the CMC and far below the CMT, we can presume that there should be a negligibly small amount of molecularly dispersed polymers in the system.

SAXS Data Analysis. Pedersen and Svaneborg's general scattering formula from polymeric micelles is given by the following expression:[33,40]

$$F(q) = N_{agg}{}^2\beta_{core}{}^2A_{core}(q)^2 + N_{agg}\beta_{chain}{}^2F_{eff}{}'(q) + 2N_{agg}{}^2\beta_{core}\beta_{chain}A_{core}(q)A_{chain}(q) + N_{agg}(N_{agg} - F_{eff}{}'(0))\beta_{chain}{}^2A_{chain}(q)^2 \quad (2)$$

where N_{agg} is the aggregation number of the micelle, β_{core} and β_{chain} are the excess scattering lengths of the core and shell chains, $A_{core}(q)$ and $A_{chain}(q)$ are the form factors of the core and PEG chain, and $F_{eff}{}'(q)$ is the effective single-chain form factor. To apply eq 2 to our analysis with the minimum adjustable parameters, eq 2 can be simplified to a great extent when $N_{agg} \gg 1$ or (> ca. 30) and the shell chains are PEG. The second term contributes much less than the others because the electron density of PEG is very close to that of water, comparing with Asp(Bzl), and thus $\beta_{core} > \beta_{chain}$. The parameter $F_{eff}{}'(q)$ is usually less than 1, and $N_{agg}(N_{agg} - F_{eff}{}'(0))$ can be assumed as $N_{agg}{}^2$. The detail of the simplification is described in the Supporting Information. Therefore, after incorporating the distribution of the size, $I(q)$ can be deduced to the following:[31]

$$\left(\frac{I(q)}{c}\right)_{c\to 0} = P(R_C)\frac{N_A}{M_w}\left\{(\rho_C - \rho_S)V_C\frac{3[\sin(qR_C) - qR_C\cos(qR_C)]}{(qR_C)^3} + 4\pi\int_{R_C}^{R_S}(\rho_S(r) - \rho_0)r^2\sin(qr)/(qr)\,dr\right\}^2 \quad (3)$$

Here, R_C and R_S are the outer radii of the core and micelle, ρ_C, $\rho_S(r)$, and ρ_0 are the scattering lengths (cm^{-1}) of the core, shell, and solvent, respectively, and N_A is the Avogadro number. $P(R_C)$ gives smearing due to the size distribution, and we assumed that the core size has a Gaussian distribution with the standard deviation of σ. In this paper, we presume the following monomer concentration dependence for $\rho_S(r)$, since the exponent of −4/3 is originally derived by Daoud and Cotton for the solvent-swollen chains in multi-armed star polymers, and later has been shown to well describe the chain statistic of the shell chain of polymeric micelles.[25]

$$\rho_S(r) = (\rho_{Shell_{inner}} - \rho_0)\left(\frac{r}{R_C}\right)^{-4/3} + \rho_0 \quad \text{for} \quad R_C < r < R_S \quad (4)$$

where $\rho_{Shell_{inner}}$ is the scattering length of the inner limit of the shell. Hereinafter, we denote the core−shell micelle that has the concentration profile of eq 4 by the "core−corona" model.

Since we used the absolute scattering intensities of water for intensity correction, the electron density (Ze: the number of electrons per unit volume) for each layer can be obtained by $\rho/r_e = Ze$, where r_e is the classical radius of the electron: 2.818×10^{-13} cm. In eq 3, M_W is given by LS in FFF and ρ_0 can be calculated to be 1.632×10^{-2} cm^{-1}. Since the scattering intensity is measured in absolute value, the remaining unknown parameters in eq 3 are ρ_C, $\rho_{Shell_{inner}}$, R_C, R_S, and σ. We determined these parameters with an iteration method described previously,[28] noting that $\rho_0 = 334r_e \ll \rho_{PEG} < 369r_e < \rho_C$ and $R_C < R_S$. The advantage to use M_W from LS and the absolute intensities for $I(q)$ is to reduce the freedom of the fitting parameters and thus to evaluate the electron densities without ambiguity.

RESULTS

Field Flow Fractionation and Static Light Scattering. An example of the applied cross-flow profile is presented in Figure 2A, and the elution fractgrams recorded with LS at 90° and RI are shown in Figure 2B for A26.9-B83.3-s. As shown in part A, after focusing, the cross-flow rate was exponentially decreased from 3 mL/min by the time that it reached 0.1 mL/min, then it was kept at 0.1 mL/min for 14 min, and finally it was decreased linearly to 0 mL/min within 1 min. FFF makes smaller particles (i.e., smaller hydrodynamic volumes) transport faster and thus elute prior to larger particles. The peak at 2.5 min was detected by RI, while there was no peak observed with LS owing to low molecular weight. This fraction

dx.doi.org/10.1021/jp300936d | J. Phys. Chem. B 2012, 116, 8241−8250

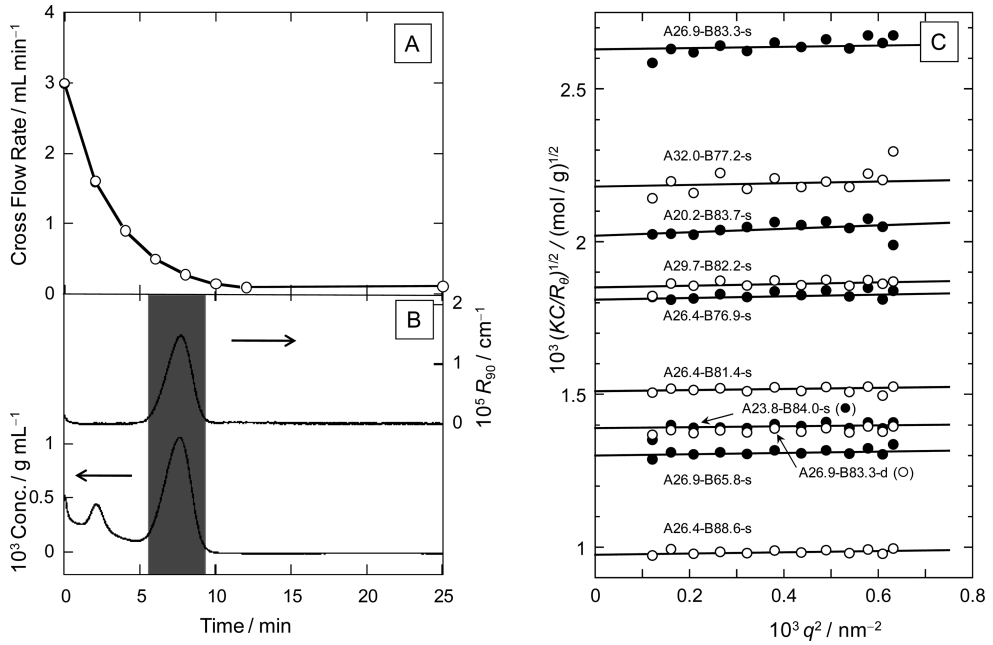

Figure 2. Field flow fractionation (FFF) and light scattering (LS) measurements. (A) An example of the cross-flow profile. (B) The resultant fractgrams detected with LS at 90° and RI (reflective index). The RI intensities were converted to concentrations. (C) The Berry plots for all samples at the top of the RI peaks.

can be assigned to either nonaggregating polymers or unreacted PEG. The peak at 8 min can be assigned to the polymeric micelles. For the micellar peak (gray area), the scattering intensity was extrapolated at $q = 0$ with the Berry plot (i.e., $(Kc/R_\theta)^{1/2}$ vs q^2), and M_w and $\langle S^2\rangle_Z$ were determined from the intercept and the slope by use of eq 1, respectively. Part C presents the Berry plots made at the peak top for each sample. The real weight-averaged molecular weight and the radius of gyration of the sample were calculated from the RI fractgram, assuming that each fraction has no distribution in mass and size. The results as well as M_n, $N_{agg,w}$, and $\partial n/\partial c$ used each analysis are summarized in Table 2, where M_n is the number-average molar mass.

Table 2. Molecular Characters Determined with Multi-Angle Light Scattering Coupled with Field-Flow Fractionation and the Aggregation Number

micelle sample code[a]	$\partial n/\partial c$[b] ($cm^3\ g^{-1}$)	$10^{-5}\ M_n$ (g mol^{-1})	$10^{-5}\ M_w$ (g mol^{-1})	$\langle S^2\rangle_Z^{1/2}$ (nm)	$N_{agg,w}$
A26.4-B76.9-s	0.162	3.78	3.82	11 ± 4	37.8
A26.4-B81.4-s	0.161	4.21	4.24	11 ± 4	41.5
A26.4-B88.6-s	0.167	10.2	10.4	12 ± 4	100.2
A20.2-B83.7-s	0.170	3.16	3.25	15 ± 5	35.8
A23.8-B84.0-s	*0.167*	4.67	4.78	9 ± 3	49.0
A29.7-B82.2-s	*0.165*	3.50	3.55	11 ± 3	32.7
A32.0-B77.2-s	0.158	3.36	3.58	12 ± 4	32.1
A26.9-B65.8-s	*0.161*	2.71	2.77	9 ± 3	27.9
A26.9-B83.3-s	0.167	7.63	7.69	12 ± 4	74.3
A26.9-B83.3-d	0.167	6.88	7.02	12 ± 3	67.9

[a]The suffixes of -s and -d stand for how to prepare the micelle: s, sonication; d, dialysis. [b]The refractive index increments were determined for each sample, except for the samples typed in italic. The values were estimated by use of the relation described in the text.

Most samples showed no additional peak on the longer elution-time side in FFF, indicating no secondary aggregation. However, a few samples, such as A26.9-B83.3-d, A26.9-B65.8-s, and A32.0-B77.2-s, showed the secondary aggregation detected in the LS fractgram as presented in the Supporting Information. In terms of the composition based on RI, the secondary aggregates are a minority component so that these aggregates could not be detectable by RI. Since there were no large aggregates in A26.9-B83.3-s containing the same polymer sample with A26.9-B83.3-d, but prepared differently, sonication seems better than dialysis to avoid secondary aggregation.

Small Angle X-ray Scattering. Figure 3 plots $[I(q)/c]_{c\to 0}$ against q for three samples—A26.4-B76.9-s, A26.4-B88.6-s, A26.4-B81.4-s—with the same DP_{Asp} but different F_{Bzl}. The plots for the other samples are presented in the Supporting Information. All of the scattering profiles show the typical

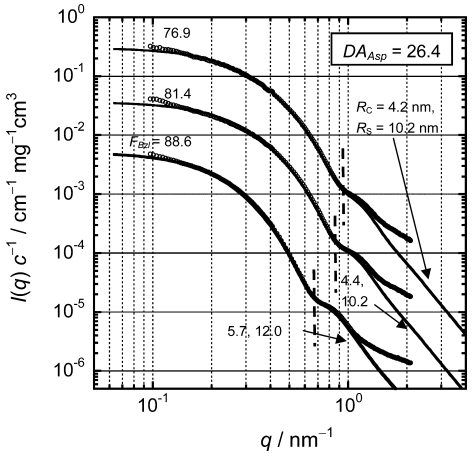

Figure 3. Comparison of the SAXS profiles for A26.4-B76.9-s, A26.4-B81.4-s, and A26.4-B88.6-s, and the theoretical values calculated from the core−corona spherical model with the indicated parameters. The dashed lines show the positions of the dent between the first and second amplitude.

dx.doi.org/10.1021/jp300936d | J. Phys. Chem. B 2012, 116, 8241−8250

Table 3. Structural Parameters Determined from SAXS with the Core−Corona Spherical Model of eq 3 and Comparison of the Radius of Gyration Determined Form the Guinier Plot

				Ze (e nm^{-3})			
sample	R_g[a] (nm)	R_c (nm)	R_s (nm)	core	shell$_{inner}$	σ/R_s	d[b] (g cm^{-3})
A26.4-B76.9-s	7.6	4.2 ± 0.1	10.2 ± 0.4	410	338	0.2	0.99
A26.4-B81.4-s	6.7	4.4 ± 0.1	10.2 ± 0.5	412	339	0.2	0.96
A26.4-B88.6-s	9.4	5.7 ± 0.1	12.0 ± 0.7	400	340	0.2	1.10
A20.2-B83.7-s	7.4	4.3 ± 0.1	10.2 ± 0.5	403	337	0.2	0.69
A23.8-B84.0-s	7.4	4.8 ± 0.1	11.5 ± 0.4	405	339	0.2	0.80
A29.7-B82.2-s	6.5	4.7 ± 0.1	11.1 ± 0.4	408	337	0.2	0.70
A32.0-B77.2-s	6.1	4.3 ± 0.1	10.2 ± 0.5	410	337	0.2	0.95
A26.9-B65.8-s	8.1	3.9 ± 0.1	9.3 ± 0.4	412	338	0.2	0.88
A26.9-B83.3-s	7.1	5.4 ± 0.1	10.2 ± 0.5	418	341	0.2	0.96
A26.9-B83.3-d	7.9	5.4 ± 0.1	11.8 ± 0.8	418	340	0.16	0.87

[a]The radius of gyration determined form the Guinier plots presented in the Supporting Information. [b]The apparent density (d) is evaluated from $N_{agg,w}$.

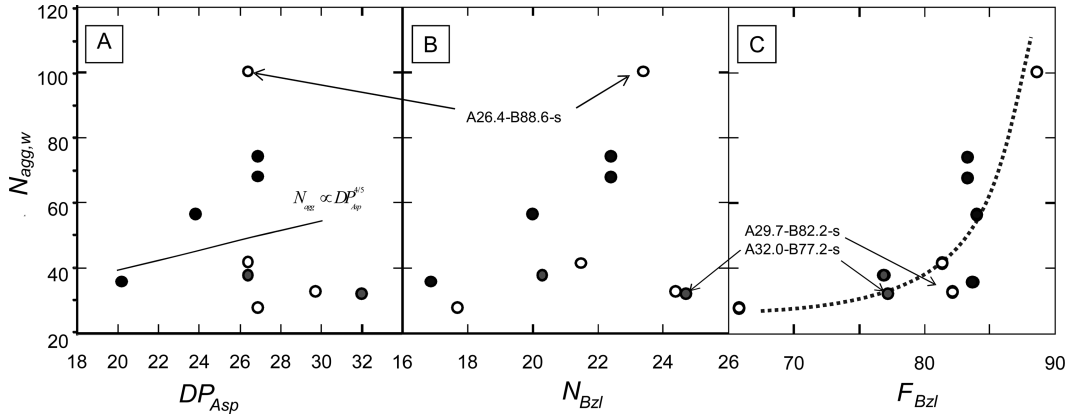

Figure 4. Correlation between the number of aggregated chains in the micelles ($N_{agg,w}$) and the degree of polymerization of the poly aspartic acid block (DP_{Asp}) in part A, and the number of the benzyl-esterified aspartic acid (N_{BzI}) in part B, and the benzylation fraction (F_{BzI}) of the P(Asp(Bzl)) block (F_{BzI}) in part C. The black filled circles are $F_{BzI} \approx 83-84$, the gray ones are $F_{BzI} \approx 77$, and the unfilled ones are for the other samples with different F_{BzI}. The relation predicted by the scaling theory is drawn as a solid line in part A.

features for spherical micelles: converging into a constant value as $q \rightarrow 0$, a drastic decrease of $I(q)$ around $q \sim 0.2-0.4$ nm^{-1}, presence of a dent indicated with the dashed line in the figure, and presence of the second amplitude at higher q. From the lower q scattering, the Guinier plot ($\ln I(q)$ vs q^2) was constructed to obtain R_g. In our setup, there was sometimes not negligible parasitic scattering observed around the beam-stopper and thus there was error involved in the Guinier plots. The resultant values are summarized in the second column of Table 3. Comparing the three samples in Figure 3, R_g increased with increasing benzylation fraction. This is consistent with the change of the position of the bent between the first and second amplitudes (the minimum position is denoted by q^*), since q^* is related to the radius for solid spheres (R) with $Rq^* = 4.493\cdots$ and the decreasing q^* with increase of the benzylation fraction means increase in R.

The best fitted lines are compared with the data in the same figure, showing good agreement between the theory and the experimental data, except for the up-turn of $I(q)$ at the lower and higher q regions. At the lower q region, as mentioned in the FFF study, some of the solutions contain small amounts of secondary aggregation. These relative large particles caused the up-turn at the small angle region. At the higher q region, as mentioned in the previous paper[28] and others, this up-turn can be ascribed to the presence of atomic- and molecular-scale orders and of the density fluctuations arising from thermal motions of atoms.[27,39]

The obtained fitting data are summarized in Table 3. In the previous paper,[27] we had to assume that the solvent did not penetrate the core and thus ρ_C is the same as that of bulk. Other papers suggested that this assumption may not be correct although a good approximation.[32] As shown here, by combination of LS and SAXS, we do not need to assume ρ_C and it can be determined rather straightforwardly from M_w and the absolute value of $[I(q)/c]_{c\rightarrow 0}$. Good contrast of the core, ρ_C, and R_C can be determined quite accurately within ±2%, while $\rho_{Shell_{inner}}$ is so close to ρ_0 that some error crept in both $\rho_{Shell_{inner}}$ and R_S. We calculated the core density defined by $d = N_{agg}M_{P(Asp(Bzl))}/N_A \div V_C$ and summarized in the same table.

DISCUSSION

Major Factors to Determine $N_{agg,w}$. Figure 4 plots $N_{agg,w}$ against three values: DP_{Asp}, N_{BzI}, and F_{BzI}. The scaling theory predicts the following relation:[20]

$$N_{agg} \propto (N_C/\varphi)^{4/5}\gamma^{6/5} \quad (5)$$

Here, γ and φ are the surface free energy per monomer caused by unfavorable interactions between water and hydrophobic chain and the volume fraction, respectively. When we use DP_{Asp} as N_C in eq 4 and constructed the $N_{agg,w}$ vs DP_{Asp} plot (part A), it is clear that eq 5 fails to describe our results. This implies that

dx.doi.org/10.1021/jp300936d | J. Phys. Chem. B 2012, 116, 8241−8250

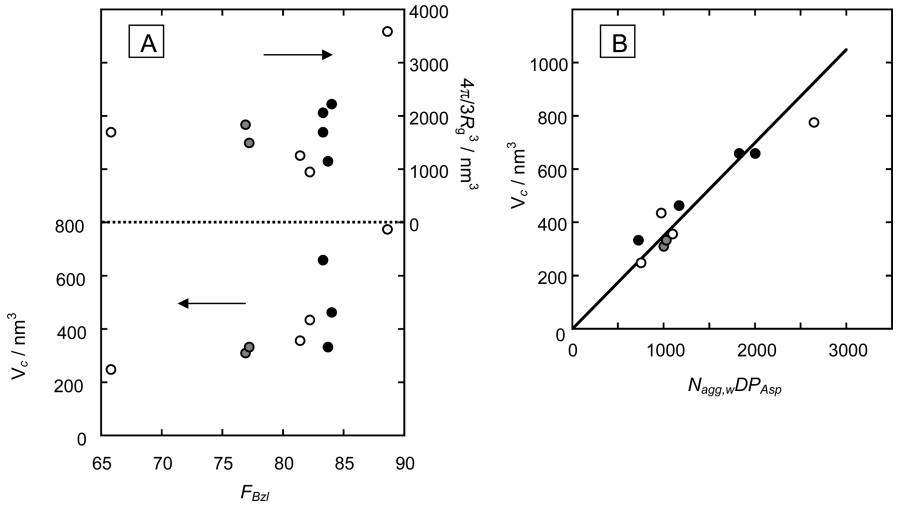

Figure 5. The benzylation faction (F_{Bzl}) dependence of the core volume calculated from $V_C = 4\pi/3R_C^3$ and of $4\pi/3R_g^3$ in part A, and V_C is plotted against $N_{agg,w} \times DP_{Asp}$ in part B. The black and gray filled circles and the unfilled circles are the same in Figure 6.

we cannot treat γ and φ as a constant. Part C presents the relation of $N_{agg,w}$ and F_{Bzl}, showing that these two parameters are well correlated, leading to F_{Bzl} being the major factor to determine $N_{agg,w}$. In part C, $N_{agg,w}$ increased with increase of F_{Bzl}. When the carboxyl group is benzyl-esterified, this moiety becomes quite hydrophobic and, in reverse, the hydrated carboxyl group is hydrophilic. Therefore, F_{Bzl} is considered to reflect the hydrophobic/hydrophilic balance of the P(Asp(Bzl)) block. Therefore, the degree of the hydrophobic interaction is the most significant factor to determine $N_{agg,w}$, even though F_{Bzl} changes in such a relatively small range (66−89 mol %). The benzyl-esterified group presumably plays two roles in the micellar formation: one is to increase the interface tension through the hydrophobic interactions (that effect is accounted for by γ), and the other is the attractive interaction between the aromatic groups due to $\pi-\pi$ stacking. The later factor is not included in the scaling theory.

In part C, the data points are rather scattered even at the same F_{Bzl}, suggesting that F_{Bzl} is not the only factor to determine $N_{agg,w}$. To compare the data having similar F_{Bzl}, the data points with $F_{Bzl} \approx 83-84$ and with $F_{Bzl} \approx 77$ are marked as the black- and gray-filled circles, respectively. In part A, for $F_{Bzl} \approx 83-84$ (black-filled), $N_{agg,w}$ increased 2-fold with an increase of DP_{Asp} by 40%, and for $F_{Bzl} \approx 77$ (gray filled), in reverse, $N_{agg,w}$ slightly decreased with increase of DP_{Asp}. If we assume invariable γ and φ for the same F_{Bzl}, $N_{agg,w}$ should be scaled by 4/5 according to eq 5 and such dependence is drawn as a thin solid line in the figure. The data points even with the same F_{Bzl} do not follow this relation. One of the reasons is the wrong assumption of constant φ, because the density (d), which is directly related to φ, is not constant as shown in Table 3. At this moment, we do not have a clear explanation for why the same F_{Bzl} did not give a similar d. It should be noted that a large difference in d between A26.9-B83.3-s and -d (the same polymer with different preparation) shows that d may depend on how the samples are made and thus ambiguity in d may be related to slow kinetics of the micellar formation, as mentioned previously.[20]

The Core Sizes. Figure 5A plots the core volume ($V_C = 4/3\pi R_C^3$) and the corresponding values from R_g. V_C increases with increase of F_{Bzl}. Again, we can conclude that F_{Bzl} is the major factor to determine the micellar architecture. R_g^3 is almost independent of F_{Bzl}, except for A26.4-B88.6-s. As mentioned previously, the parasitic scattering causes large error in the Guinier plot when determining R_g. These errors should obscure the relation between F_{Bzl} and R_g. Figure 5B plots V_C vs $N_{agg,w} \times DP_{Asp}$. Since the relation of $N_{agg,w} \propto V_C\varphi/DP_{Asp}$ should hold anytime, all of the data points would be on one straight line crossing the origin when φ is constant. Although there is a good correlation between the two parameters with a correlation coefficient of 0.35, the data points are scattered along the line. This indicates that φ is not constant.

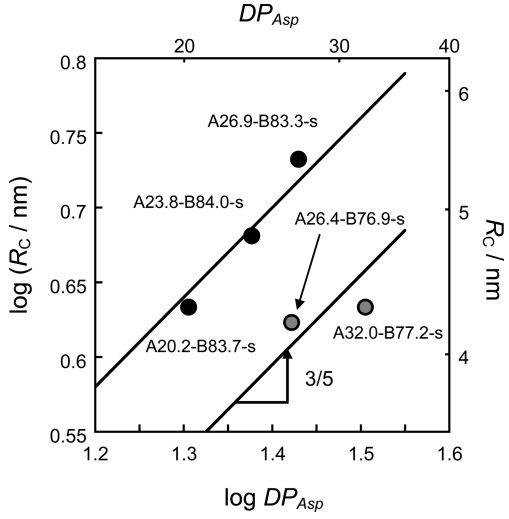

Figure 6. DP_{Asp} dependence of R_C for the same F_{Bzl}.

Figure 6 double-logarithmically plots R_C against DP_{Asp} for $F_{Bzl} \approx 83-84$ and with $F_{Bzl} \approx 77$, comparing the theoretical prediction:[20]

$$R_C \propto a_C\left(\frac{N_C}{\varphi}\right)^{3/5}\gamma^{2/5} \quad (6)$$

where a_C is the size of the monomer related to the Kuhn segment length and the molecular diameter. The experimental data points are well scaled with the same slope as the theory for both cases, although we do not know why R_C follows the

dx.doi.org/10.1021/jp300936d | J. Phys. Chem. B 2012, 116, 8241−8250

prediction but $N_{agg,w}$ does not. This agreement shows that, if DP_{Asp} is same, it is safe to presume that the size of the core is determined by the balance of the elastic free energy of the core chain, the interfacial free energy, and the conformational free energy of the shell chain. In eq 6, the difference in the hydrophobicity of the core chains is accounted for by γ and the importance of γ in the micellar architecture has been experimentally shown.[41] Assuming a_C is independent of F_{Bzl}, it can be estimated that γ increased by twice by changing F_{Bzl} from 77 to 83−84.

PEG Chain Crowding. How the tethered chains are crowding on the flat surface can be described by the chain density reduced by πR_g^2, where R_g is the radius of gyration of the isolated chain at its unperturbed state.[42] When this index is less than 4, the tethered chains are not interacting with each other (called mushroom region). For 4−10, the chains are crossed over with each other and the conformation of each chain is deviated from the sphere (called the brush region). In the range of >10, the chains are highly stretched normal to the surface. Svaneborg et al. extended this concept to the shell of polymeric micelles, and the reduced chain density is given by[43]

$$\sigma_{PEG} = \frac{N_{agg}\pi R_{g,PEG}^{\ 2}}{4\pi(R_C + R_{g,PEG})^2} \tag{7}$$

where $R_{g,PEG}$ is the radius of gyration of the PEG single chain, in our case $R_{g,PEG}$ = 3 nm with $M_w \sim 5000$. The obtained value of σ_{PEG} increases with increments of $N_{agg,w}$ from 1.3 to 3, as illustrated in Figure 7. The magnitude of σ_{PEG} suggests that the

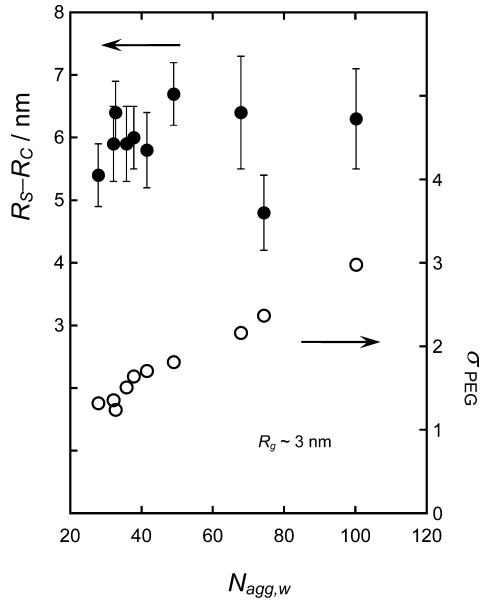

Figure 7. $N_{agg,w}$ dependence of the PEG layer thickness R_S−R_C and the reduced surface coverage σ_{PEG} defined by eq 7.

shell PEG chains slightly contact with each other but are not stretched like those in the brush region. The PEG layer thicknesses are about 6 nm for all samples. This value is approximately the same as $2R_{g,PEG}$ (=6 nm), confirming the conclusion from σ_{PEG}. The value of $\rho_{Shell_{inner}}$ is reflecting the PEG monomer density at the core−shell interface. When we compared $\rho_{Shell_{inner}}$ with that of the unperturbed PEG chain, the former is about 1.3−2.9 times larger than the latter. Furthermore, the graft density of the PEG of the interface was about 0.17 chains/nm^2 and increased from 0.12 to 0.25 with increasing $N_{agg,w}$. These two values indicate that the PEG chains at the vicinity of the interface are rather crowded.

PEG Layer Thickness. The scaling theory predicts the following relation:[20]

$$R_S - R_C \propto \left(\frac{N_C}{\varphi}\right)^{1/5} \gamma^{3/10} \tag{8}$$

Combining eqs 5 and 8, we obtained $R_S - R_C \propto N_{agg}^{1/4}$ by ignoring other parameters. Figure 8 plots $R_S - R_C$ against $N_{agg,w}$

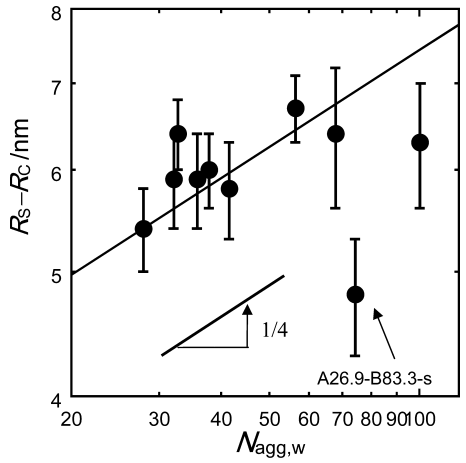

Figure 8. The tethered PEG layer thickness plotted against $N_{agg,w}$, compared with the theoretically predicted slope of 1/4.

for all of the data points as well as the slope of 1/4. The comparison shows that there is no contradiction between the data and the theory, indicating that the PEG chains are approximately described by this model. Equation 5 fails to describe the data as presented in Figure 5A, and we consider that the main reason for this failure is the relatively large variation in the core density as presented in Table 3, which is related to φ. After combining eqs 5 and 8, we obtained $R_S - R_C \propto N_{agg}^{1/4}$; i.e., the contribution from the core density and the surface free energy are eliminated. We presume that this is the reason that the PEG layer thickness is fitted by the theory.

We examined the PEG layer thickness with a planar model described by Halperin et al,[44,45] assuming that if the core size is large enough, the shell could be regarded as a planar disk. As shown in the Supporting Information, however, this model is not appropriate to describe our system.

CONCLUSIONS

Nine samples of PEG-P(Asp(Bzl)) with different benzylation fractions and aspartic chain lengths were synthesized and served for FFF/MALS and synchrotron SAXS measurements. From LS, the molar masses were determined, from which $N_{agg,w}$ was determined for each sample. The scattering profiles of SAXS could be well fitted with a core−corona spherical model. Combining the $M_W$obtained from LS, we could determine the four structural parameters R_C, R_S, ρ_C, and $\rho_{Shell_{inner}}$ without assumption. The major factor to determine $N_{agg,w}$ and R_C is found to be F_{Bzl}: the hydrophobic nature of the core. When we compared the data for the same F_{Bzl}, the scaling theory is consistent with the N_C (i.e., the core chain length) dependence of both core and micelle sizes. For the crowding nature of the

dx.doi.org/10.1021/jp300936d | J. Phys. Chem. B 2012, 116, 8241−8250

PEG, PEG chains are somehow crowded compared with in dilute solution but not highly stretched.

■ ASSOCIATED CONTENT

Supporting Information

The theoretical details of the core−corona spherical model, determination of the absolute scattering intensity and Guinier plot of SAXS, FFF chart of each micelle, SAXS profiles with theoretical curves, comparison of core−corona spherical model vs double-layer spherical model, and discussion about PEG layer thickness with planar model. This material is available free of charge via the Internet at http://pubs.acs.org.

■ AUTHOR INFORMATION

Corresponding Author

*E-mail: sakurai@kitakyu-u.ac.jp.

Notes

The authors declare no competing financial interest.

■ ACKNOWLEDGMENTS

This work is financially supported by JST CREST program and all SAXS measurements were carried out at SPring-8 40B2 (2009A0012, 2009B1397, 2010A1089, 2010B1726).

■ LIST OF ABBREVIATIONS

N_{agg}, $N_{agg,w}$: aggregation number of the micelle; substitution w means "weight average"
DP_{Asp}: degree of polymerization of the poly aspartic acid (including both benzyl-esterified and hydrated ones); this value is related to N_C, but they have different physical meanings, since the Kuhn length would be changed upon the change of the benzylation fraction of the block
R_e: Gaussian end-to-end distance of the chain of individual hydrophobic block
N_C: chain length of hydrophobic blocks
N_S: chain length of the hydrophilic blocks
N_{Bzl}: number of the benzyl-esterified aspartic acid
F_{Bzl}: benzylation fraction of the P(Asp(Bzl)) block (R_{Bzl})
$\langle S^2 \rangle_Z^{1/2}$: Z-average radius of gyration from light scattering
M_w: weight average molar mass of an aggregated micelle
K: optical constant
c: concentration of a micellar solution
R_θ: reduced scattering intensity at scattering angle 2θ
q: magnitude of the scattering vector
$\partial n/\partial c$: specific reflective index
$M_{PEG\text{-}P(Asp(Bzl))}$: molecular mass of the one PEG-P(Asp(Bzl)) chain
$I(q)$: scattering intensity of scattering vector q
β_{core}: excess scattering length of the core
β_{chain}: excess scattering length of shell chains
$A_{core}(q)$: form factors of the core
$A_{chain}(q)$: form factors of PEG chain
$F_{eff}'(q)$: effective single-chain form factor
R_C: radius of core
R_S: radius of micelle
ρ_C: scattering length of the core
$\rho_S(r)$: scattering length of the shell
ρ_0: scattering length of the solvent
r: distance from the center of the core
N_A: Avogadro number
$P(R_C)$: size distribution with Gauss function
σ: standard deviation of the size distribution
$\rho_{Shell_{inner}}$: scattering length of the inner limit of the shell
r_e: classical radius of the electron (2.818×10^{-13} cm)
Ze: number of electrons of a chemical per unit volume
M_n: number average molar mass of an aggregated micelle
R_g: radius of gyration from SAXS
d: density of the hydrophobic core
$M_{P(Asp(Bzl))}$: molecular weight of the hydrophobic block of the polymer
γ: surface free energy per monomer caused by unfavorable interactions between water and hydrophobic chain
φ: volume fraction of the core chains
V_C: volume of core ($V_C = 4/3\pi R_C^3$)
a_C: size of the monomer related with Kuhn segment length
σ_{PEG}: reduced chain density of core−shell interface
$R_{g,PEG}$: radius of gyration of the PEG isolated chain
Terminology of "core−shell" and "core−corona": Micelles are depicted as concentric spherical double layers, and such a structure is sometimes called "core−shell". In this model, the shell chain monomer concentration can be constant or decrease as it goes outside. For polymeric micelles, the later model should be appropriate (see Figure S6, Supporting Information). In this paper, when we want to emphasize such a decreasing monomer concentration, we denote "core−corona".

■ REFERENCES

(1) Aliabadi, M.; Lavasanifar, A. *Expert Opin. Drug Delivery* **2006**, *3* (1), 139.
(2) Riess, G. *Prog. Polym. Sci.* **2003**, *28* (7), 1107−1170.
(3) Nagasaki, Y.; Okada, T.; Scholz, C.; Iijima, M.; Kato, M.; Kataoka, K. *Macromolecules* **1998**, *31* (5), 1473−1479.
(4) Zhang, L.; Chan, J. M.; Gu, F. X.; Rhee, J.-W.; Wang, A. Z.; Radovic-Moreno, A. F.; Alexis, F.; Langer, R.; Farokhzad, O. C. *ACS Nano* **2008**, *2* (8), 1696−1702.
(5) Farinha, J. P. S.; d'Oliveir, J. M. R.; Martinho, J. M. G.; Xu, R.; Winnik, M. A. *Langmuir* **1998**, *14* (9), 2291−2296.
(6) Liu, X.; Kim, J.-S.; Wu, J.; Eisenberg, A. *Macromolecules* **2005**, *38* (16), 6749−6751.
(7) Shen, H.; Zhang, L.; Eisenberg, A. *J. Am. Chem. Soc.* **1999**, *121* (12), 2728−2740.
(8) Yu, K.; Bartels, C.; Eisenberg, A. *Macromolecules* **1998**, *31* (26), 9399−9402.
(9) Yu, K.; Eisenberg, A. *Macromolecules* **1998**, *31* (11), 3509−3518.
(10) Yu, Y.; Eisenberg, A. *J. Am. Chem. Soc.* **1997**, *119* (35), 8383−8384.
(11) Antonietti, M.; Heinz, S.; Schmidt, M.; Rosenauer, C. *Macromolecules* **1994**, *27* (12), 3276−3281.
(12) Yokoyama, M.; Kwon, G. S.; Okano, T.; Sakurai, Y.; Ekimoto, H.; Okamoto, K.; Mashiba, H.; Seto, T.; Kataoka, K. *Drug Delivery* **1993**, *1*, 11−19.
(13) Harada, A.; Kataoka, K. *Macromolecules* **1998**, *31* (2), 288−294.
(14) Kataoka, K.; Harada, A.; Nagasaki, Y. *Adv. Drug Delivery Rev.* **2001**, *47* (1), 113−131.
(15) Kabanov, A. V.; Batrakova, E. V.; Alakhov, V. Y. *J. Controlled Release* **2002**, *82* (2−3), 189−212.
(16) Vinogradov, S.; Batrakova, E.; Li, S.; Kabanov, A. *Bioconjugate Chem.* **1999**, *10* (5), 851−860.
(17) Matsumura, Y. *Adv. Drug Delivery Rev.* **2008**, *60*, 899−914.
(18) Yokoyama, M. *Expert Opin. Drug Delivery* **2010**, *7*, 145−158.
(19) Yamamoto, T.; Yokoyama, M.; Opanasopit, P.; Hayama, A.; Kawano, K.; Maitani, Y. *J. Controlled Release* **2007**, *123* (1), 11−18.
(20) Zhulina, E. B.; Adam, M.; LaRue, I.; Sheiko, S. S.; Rubinstein, M. *Macromolecules* **2005**, *38* (12), 5330−5351.
(21) Zhulina, E. B.; Birshtein, T. M. *Polym. Sci. USSR* **1985**, *27*, 570.
(22) Hamley, I. W. *The Physics of Block Copolymers*; Oxford University Press: Oxford, U.K., 1998.

(23) Halperin, A.; Alexander, S. *Macromolecules* **1987**, *20* (5), 1146−1152.
(24) de Gennes, P. G. *Scaling Concepts in Polymer Physics*; Cornell University Press: Ithaca, NY, 1979.
(25) Daoud, D.; Cotton, J. P. *J. Phys.* **1982**, *43*, 531−538.
(26) Riley, T.; Heald, C. R.; Stolnik, S.; Garnett, M. C.; Illum, L.; Davis, S. S.; King, S. M.; Heenan, R. K.; Purkiss, S. C.; Barlow, R. J.; Gellert, P. R.; Washington, C. *Langmuir* **2003**, *19* (20), 8428−8435.
(27) Akiba, I.; Terada, N.; Hashida, S.; Sakurai, K.; Sato, T.; Shiraishi, K.; Yokoyama, M.; Masunaga, H.; Ogawa, H.; Ito, K.; Yagi, N. *Langmuir* **2010**, *26* (10), 7544−7551.
(28) Higgins, J. S.; Benoît, H. C. *Polymers and Neutron Scattering*; Oxford University Press: Oxford, U.K., 1994.
(29) Koga, T.; Tanaka, F.; Motokawa, R.; Koizumi, S.; Winnik, F. o. M. *Macromolecules* **2008**, *41* (23), 9413−9422.
(30) Nakano, M.; Deguchi, M.; Matsumoto, K.; Matsuoka, H.; Yamaoka, H. *Macromolecules* **1999**, *32* (22), 7437−7443.
(31) Nakano, M.; Matsumoto, K.; Matsuoka, H.; Yamaoka, H. *Macromolecules* **1999**, *32* (12), 4023−4029.
(32) Nakano, M.; Matsuoka, H.; Yamaoka, H.; Poppe, A.; Richter, D. *Macromolecules* **1999**, *32* (3), 697−703.
(33) Pedersen, J. S.; Svaneborg, C.; Almdal, K.; Hamley, I. W.; Young, R. N. *Macromolecules* **2003**, *36* (2), 416−433.
(34) Sommer, C.; Pedersen, J. S. *Macromolecules* **2004**, *37* (5), 1682−1685.
(35) Yokoyama, M.; Fukushima, S.; Uehara, R.; Okamoto, K.; Kataoka, K.; Sakurai, Y.; Okano, T. *J. Controlled Release* **1998**, *50*, 79−92.
(36) Naruse, K.; Eguchi, K.; Akiba, I.; Sakurai, K.; Masunaga, H.; Ogawa, H.; Fossey, J. S. *J. Phys. Chem. B* **2009**, *113* (30), 10222−10229.
(37) Eguchi, K.; Kaneda, I.; Hiwatari, Y.; Masunaga, H.; Sakurai, K. *J. Appl. Crystallogr.* **2007**, *40* (s1), s264−s268.
(38) Orthaber, D.; Bergmann, A.; Glatter, O. *J. Appl. Crystallogr.* **2000**, *33* (2), 218−225.
(39) Roe, R. J. *Methods of X-ray and Neutron Scattering in Polymer Science*; Oxford University Press: Oxford, U.K., 2000.
(40) Choi, S.-H.; Bates, F. S.; Lodge, T. P. *J. Phys. Chem. B* **2009**, *113* (42), 13840−13848.
(41) Lund, R.; Willner, L.; Stellbrink, J.; Radulescu, A.; Richter, D. *Macromolecules* **2004**, *37* (26), 9984−9993.
(42) Chen, W. Y.; Zheng, J. X.; Cheng, S. Z. D.; Li, C. Y.; Huang, P.; Zhu, L.; Xiong, H.; Ge, Q.; Guo, Y.; Quirk, R. P.; Lotz, B.; Deng, L.; Wu, C.; Thomas, E. L. *Phys. Rev. Lett.* **2004**, *93* (2), 028301.
(43) Svaneborg, C.; Pedersen, J. S. *Macromolecules* **2002**, *35* (3), 1028−1037.
(44) Halperin, A.; Tirrell, M.; Lodge, T. *Tethered chains in polymer microstructures Macromolecules: Synthesis, Order and Advanced Properties*. Springer: Berlin/Heidelberg, 1992; Vol. *100*, pp 31−71.
(45) Schneider, C.; Jusufi, A.; Farina, R.; Li, F.; Pincus, P.; Tirrell, M.; Ballauff, M. *Langmuir* **2008**, *24* (19), 10612−10615.